

**STRUCTURAL, MORPHOLOGICAL AND OPTICAL
PROPERTIES OF BIMETALLIC NANOPARTICLES
IN TELLURITE GLASS SYSTEM FOR
IMPROVEMENT IN SURFACE-ENHANCED
RAMAN SCATTERING**



IXORA FERODOLIN

UMS
UNIVERSITI MALAYSIA SABAH

**FACULTY OF SCIENCE AND NATURAL
RESOURCES
UNIVERSITI MALAYSIA SABAH
2020**

**STRUCTURAL, MORPHOLOGICAL AND OPTICAL
PROPERTIES OF BIMETALIC NANOPARTICLES
IN TELLURITE GLASS SYSTEM FOR
IMPROVEMENT IN SURFACE-ENHANCED
RAMAN SCATTERING**

IXORA FERODOLIN



**THIS IS SUBMITTED IN FULFILLMENT OF THE
REQUIREMENTS FOR THE DEGREE
OF MASTER OF SCIENCE**

**FACULTY OF SCIENCE AND NATURAL
RESOURCES
UNIVERSITI MALAYSIA SABAH
2020**

UNIVERSITI MALAYSIA SABAH

BORANG PENGESAHAN STATUS TESIS

JUDUL : **STRUCTURAL, MORPHOLOGICAL AND OPTICAL PROPERTIES OF BIMETALLIC NANOPARTICLES IN TELLURITE GLASS SYSTEM FOR IMPROVEMENT IN SURFACE-ENHANCED RAMAN SCATTERING**

IJAZAH : **SARJANA SAINS**

BIDANG : **FIZIK DENGAN ELEKTRONIK**

Saya **IXORA FERODOLIN**, Sesi **2018-2020**, mengaku membenarkan tesis Sarjana ini disimpan di Perpustakaan Universiti Malaysia Sabah dengan syarat-syarat kegunaan seperti berikut:-

1. Tesis ini adalah hak milik Universiti Malaysia Sabah
2. Perpustakaan Universiti Malaysia Sabah dibenarkan membuat salinan untuk tujuan pengajian sahaja.
3. Perpustakaan dibenarkan membuat salinan tesis ini sebagai bahan pertukaran antara institusi pengajian tinggi.
4. Sila tandakan (/):

SULIT

(Mengandungi maklumat yang berdarjah keselamatan atau kepentingan Malaysia seperti yang termaktub di dalam AKTA RAHSIA 1972)

TERHAD

(Mengandungi maklumat TERHAD yang telah ditentukan oleh organisasi/badan di mana penyelidikan dijalankan)

TIDAK TERHAD

Disahkan Oleh,

IXORA FERODOLIN
MS1721045T

(Tandatangan Pustakawan)

Tarikh : 10 November 2020

(Dr. Asmahani Awang)
Penyelia Utama

DECLARATION

I hereby declare that the work presented in this thesis entitled "Structural, Morphological and Optical Properties of Bimetallic Nanoparticles in Tellurite Glass System for Improvement in Surface-Enhanced Raman Scattering" is of my own effort, except for the materials, excerpts and equations referred to as cited in the reference section.

2 October 2020

Ixora Ferodolin

MS1721045T



UMS
UNIVERSITI MALAYSIA SABAH

CERTIFICATION

NAME : **IXORA FERODOLIN**
MATRIC NO : **MS1721045T**
TITLE : **STRUCTURAL, MORPHOLOGICAL AND OPTICAL
PROPERTIES OF BIMETALLIC NANOPARTICLES IN
TELLURITE GLASS SYSTEM FOR IMPROVEMENT IN
SURFACE-ENHANCED RAMAN SCATTERING**
DEGREE : **MASTER OF SCIENCE
(PHYSICS WITH ELECTRONICS)**
VIVA DATE : **17th JULY 2020**

CERTIFIED BY;

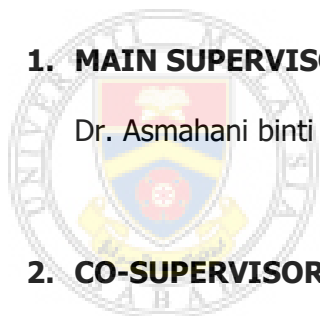
1. MAIN SUPERVISOR

Dr. Asmahani binti Awang

2. CO-SUPERVISOR

Assoc. Prof. Dr. Jedol Dayou

Signature



UMS
UNIVERSITI MALAYSIA SABAH

ACKNOWLEDGEMENT

This thesis existence owes to people who have helped me since from the start of my research work. First and foremost, I would like to express my gratitude and appreciation to my supervisor, Dr. Asmahani binti Awang, and my co-supervisor, Assoc. Prof. Dr. Jedol Dayou, for their countless guidance, kind support, as well as to keep engaging me with new ideas and beneficial suggestions throughout the whole process to carry out my research work with quality of work.

My sincere gratitude as well goes to every of the lab assistants who have guiding me with the uses of instrumentation in the laboratory in order to carry out the characterization of my samples. Special thanks go to the rest of my fellow seniors, for their endless support as well as always being around accomplishing our master research work together through days and nights.

Lastly, big thanks go to both of my loving and supportive parents for always providing me with everything I need, for nurturing me the whole years with their endless care and love.

IXORA FERODOLIN

2 October 2020



UMS
UNIVERSITI MALAYSIA SABAH

ABSTRACT

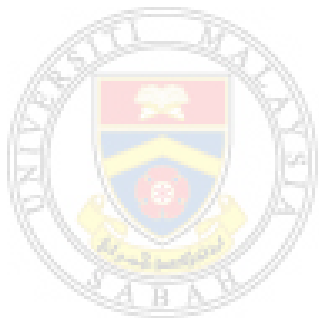
Combining bimetallic nanoparticles (NPs) with rare-earth ions in tellurite glass is an interesting field for researchers due to the amplification in surface-enhanced Raman scattering (SERS). To ensure the SERS effect to occur, a selection of SERS substrate is very crucial as their plasmonic properties and nanostructured metallic surface will stimulate the plasmonic excitation for Raman scattering to take place. Determining the SERS enhancement in tellurite glass with addition of bimetallic NPs is the main focus of this research. Four series of glass are prepared via melt-quenching method. Glass containing monometallic titanium NPs with erbium content are prepared with composition of $(70-x-y)\text{TeO}_2-20\text{ZnO}-9\text{Na}_2\text{O}-1\text{Er}_2\text{O}_3-(x)\text{TiO}_2-(y)\text{Al}_2\text{O}_3$, where $x = 0.0, 0.1, 0.2, 0.3, 0.4$ and 0.5 mol% and $y = 0$ mol%. Glass containing monometallic titanium NPs without erbium content are prepared with composition of $(70-x-y)\text{TeO}_2-20\text{ZnO}-9\text{Na}_2\text{O}-0\text{Er}_2\text{O}_3-(x)\text{TiO}_2-(y)\text{Al}_2\text{O}_3$, where $x = 0.0, 0.1, 0.2, 0.3, 0.4$ and 0.5 mol% and $y = 0$ mol%. In contrary, glass containing bimetallic titanium and aluminium NPs with erbium content are prepared with composition of $(70-x-y)\text{TeO}_2-20\text{ZnO}-9\text{Na}_2\text{O}-1\text{Er}_2\text{O}_3-(x)\text{TiO}_2-(y)\text{Al}_2\text{O}_3$ where $x = 0.0$ and 0.3 mol% and $y = 0.0, 0.1, 0.2, 0.3, 0.4, 0.5$ and 0.6 mol%. Glass containing bimetallic titanium and aluminium NPs without erbium content are prepared with composition of $(70-x-y)\text{TeO}_2-20\text{ZnO}-9\text{Na}_2\text{O}-0\text{Er}_2\text{O}_3-(x)\text{TiO}_2-(y)\text{Al}_2\text{O}_3$ where $x = 0.0$ and 0.3 mol% and $y = 0.0, 0.1, 0.2, 0.3, 0.4, 0.5$ and 0.6 mol%. In-depth characterization are performed by using X-Ray Diffraction (XRD), Ultraviolet-Visible Spectroscopy (UV-VIS) Fourier-Transform Infrared Spectroscopy (FTIR), Transmission Electron Microscopy (TEM), Photoluminescence Spectroscopy (PL), Atomic Force Microscopy (AFM) and Raman Spectroscopy. XRD spectra confirms the amorphous nature of glass samples with the appearance of broad hump between 25° to 35° and the absence of sharp peak. A weak plasmon band is observed at 550 nm for glass containing monometallic titanium NPs. Meanwhile, a weak plasmon band is observed at 554 nm and 827 nm for glass containing bimetallic titanium and aluminium NPs. The variations in the direct optical band gap, indirect optical band gap and Urbach energy is due to the contribution of metallic NPs. FTIR spectra shows the appearance of Zn-O tetrahedral bond, symmetric stretching vibrations of Te-O in Te, Te-O-Zn linkages, vibrations of water molecules and fundamental stretching of hydroxyl group for glass containing monometallic NPs. Glass containing bimetallic NPs display the Zn-O tetrahedral bond, stretching vibrations of Al-O, Te-O bending vibrations in TeO_3 units, Al-O stretching, vibrations of water molecules and fundamental stretching of hydroxyl group. TEM image display the increasing size of NPs following the Ostwald ripening process and coalescence process. AFM image illustrates the formation of scattered island due to NPs. PL emission spectra display the two significant peaks centred at 547 nm and 668 nm with enhancement in intensity due to the surface plasmon resonance (SPR) effect. Raman spectra illustrate the amplification in Raman signal with Raman enhancement factor of $1.55, 1.45, 1.51$ and 1.61 for TZNETiAl0.6 glass. The amplification in Raman signal due to excitations of surface plasmon from titanium and aluminium NPs. TZNETiAl0.6 glass shows optimum properties to be used in molecular detection application due to favourable surface roughness value which is suitable for substrate properties and highest enhancement intensity in PL and Raman spectra attribute to the plasmonic effect from titanium and aluminium NPs.

ABSTRAK

SIFAT STRUKTUR, MORFOLOGI DAN OPTIK ZARAHNANO DWILOGAM DALAM SISTEM KACA TELURIT UNTUK KESAN PENINGKATAN PENYERAKAN PERMUKAAN RAMAN

Gabungan zarahnano dwilogam dengan ion nadir bumi dalam kaca telurit adalah bidang kaji yang menarik bagi para penyelidik disebabkan kesan peningkatan penyerakan permukaan Raman (SERS). Untuk memastikan kesan SERS berlaku, pemilihan substratum SERS adalah sangat penting di mana sifat plasmonik dan struktur permukaan logam nano akan membantu dalam pengujian plasmonik untuk penyerakan Raman. Penentuan peningkatan penyerakan permukaan Raman dalam kaca telurit dengan penambahan zarahnano dwilogam ialah fokus utama dalam kajian ini. Empat siri kaca disediakan melalui kaedah perlindungan leburan. Kaca mengandungi monologam zarahnano titanium dengan kandungan erbium disediakan dengan komposisi $(70-x-y)\text{TeO}_2-20\text{ZnO}-9\text{Na}_2\text{O}-1\text{Er}_2\text{O}_3-(x)\text{TiO}_2-(y)\text{Al}_2\text{O}_3$, di mana $x = 0.0, 0.1, 0.2, 0.3, 0.4$ dan 0.5 mol% dan $y = 0$ mol%. Kaca mengandungi monologam zarahnano titanium tanpa kandungan erbium disediakan dengan komposisi $(70-x-y)\text{TeO}_2-20\text{ZnO}-9\text{Na}_2\text{O}-0\text{Er}_2\text{O}_3-(x)\text{TiO}_2-(y)\text{Al}_2\text{O}_3$, di mana $x = 0.0, 0.1, 0.2, 0.3, 0.4$ dan 0.5 mol% dan $y = 0$ mol%. Sebaliknya, kaca mengandungi dwilogam zarahnano titanium dan aluminium dengan kandungan erbium disediakan dengan komposisi $(70-x-y)\text{TeO}_2-20\text{ZnO}-9\text{Na}_2\text{O}-1\text{Er}_2\text{O}_3-(x)\text{TiO}_2-(y)\text{Al}_2\text{O}_3$ di mana $x = 0.0$ dan 0.3 mol% dan $y = 0.0, 0.1, 0.2, 0.3, 0.4, 0.5$ dan 0.6 mol%. Kaca mengandungi dwilogam zarahnano titanium dan aluminium tanpa kandungan erbium disediakan dengan komposisi $(70-x-y)\text{TeO}_2-20\text{ZnO}-9\text{Na}_2\text{O}-0\text{Er}_2\text{O}_3-(x)\text{TiO}_2-(y)\text{Al}_2\text{O}_3$ di mana $x = 0.0$ dan 0.3 mol% dan $y = 0.0, 0.1, 0.2, 0.3, 0.4, 0.5$ dan 0.6 mol%. Pencirian lanjut dijalankan menggunakan Pembelauan Sinar-X (XRD), Spektroskopi Ultraungu-Cahaya Nampak (UV-VIS), Spektroskopi Inframerah Transformasi Fourier (FTIR), Mikroskopi Penghantaran Elektron (TEM), Spektroskopi Pendarkilau (PL), Mikroskopi Daya Atom (AFM) dan Spektroskopi Raman. Spektra XRD mengesahkan sifat amorfus sampel kaca dengan kemunculan bonggol pada 25° sehingga 35° dan ketidakhadiran puncak tajam. Kepelbagaian pada jurang jalur optik langsung, jurang jalur optik tak langsung dan tenaga Urbach disebabkan sumbangan zarahnano logam. Jalur plasmon lemah didapati pada 550 nm bagi kaca mengandungi monologam zarahnano titanium. Manakala, jalur plasmon lemah didapati pada 554 nm dan 827 nm bagi kaca mengandungi dwilogam zarahnano titanium dan aluminium. Kepelbagaian pada jurang jalur optik langsung, jurang jalur optik tak langsung dan tenaga Urbach disebabkan sumbangan zarahnano logam. Spektra FTIR menunjukkan kemunculan ikatan tetrahedron Zn-O, getaran regangan simetri Te-O pada Te, rantaian Te-O-Zn, getaran molekul air dan regangan asas kumpulan hidroksil bagi kaca mengandungi zarahnano monologam. Kaca yang mengandungi zarahnano dwilogam menunjukkan ikatan tetrahedron Zn-O, getaran regangan Al-O, getaran lengkungan Te-O dalam unit TeO_3 , regangan Al-O, getaran molekul air dan regangan asas kumpulan hidroksil. Imej TEM menunjukkan peningkatan saiz zarahnano melalui proses pematangan Ostwald dan proses pergabungan. Imej AFM menunjukkan pembentukan serakan pulau-pulau disebabkan zarahnano. Spektra sinaran PL menunjukkan dua puncak ketara berpusat pada 547 nm dan 668 nm dengan peningkatan pada keamatan disebabkan kesan resonans plasmon permukaan (SPR).

Spektra Raman menunjukkan penggandaan pada isyarat Raman dengan faktor peningkatan 1.55, 1.45, 1.51 dan 1.61 bagi kaca TZNETiAlO.6. Penggandaan pada isyarat Raman disebabkan pengujaan plasmon permukaan daripada zarahnano titanium dan aluminium. Kaca TZNETiAlO.6 menunjukkan ciri-ciri optimum untuk digunakan dalam aplikasi pengesanan molekul disebabkan nilai kekasaran permukaan yang sesuai untuk dijadikan sebagai sifat substrat dan peningkatan keamatan tertinggi pada spektra PL dan Raman disebabkan oleh kesan plasmonik daripada zarahnano titanium dan aluminium.



UMS
UNIVERSITI MALAYSIA SABAH

TABLE OF CONTENTS

	Page
TITLE	i
DECLARATION	ii
CERITIFICATION	iii
ACKNOWLEDGEMENT	iv
ABSTRACT	v
<i>ABSTRAK</i>	vi
TABLE OF CONTENTS	viii
LIST OF TABLES	xi
LIST OF FIGURES	xiii
LIST OF ABBREVIATIONS	xvii
LIST OF SYMBOLS	xviii
LIST OF APPENDIX	xix
CHAPTER 1: INTRODUCTION	1
1.1 Background of Study	1
1.2 Problem Statement	3
1.3 Objectives	4
1.4 Scope of Study	4
1.5 Research Significant	5
1.6 Research Outline	6
CHAPTER 2: LITERATURE REVIEW	8
2.1 Introduction	8
2.2 Early Glass Formation	8
2.3 The Glass Transition	9
2.4 Tellurite-Based Glass	11
2.4.1 The Network Former and Modifier	13
2.4.2 Rare Earth Ions	15
2.5 Metallic Nanoparticles	17
2.5.1 Monometallic Nanoparticles	18

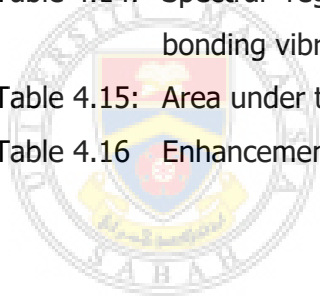
2.2.2	Bimetallic Nanoparticles	19
2.6	Growth of Metallic Nanoparticles	21
2.6.1	Ostwald Ripening Process	21
2.6.2	Coalescence Process	23
2.7	Surface Plasmon Resonance	23
2.8	Glass as SERS Substrate	24
2.9	Structural Properties	26
2.9.1	X-Ray Diffraction (XRD)	26
2.9.2	Fourier-Transform Infrared Spectroscopy (FTIR)	29
2.9.3	Surface-Enhanced Raman Scattering (SERS)	32
2.9.4	Atomic Force Microscopy (AFM)	35
2.9.5	Transmission Electron Microscopy (TEM)	39
2.10	Optical Properties	41
2.10.1	Ultraviolet-Visible (UV-VIS) Spectroscopy	41
2.10.2	Photoluminescence (PL) Spectroscopy	46
	CHAPTER 3: METHODOLOGY	49
3.1	Introduction	49
3.2	Glass Fabrication	49
3.3	Structural Characterization	52
3.3.1	X-Ray Diffraction (XRD) Spectroscopy	53
3.3.2	Fourier-Transform Infrared Spectroscopy (FTIR)	54
3.3.3	Transmission Electron Microscopy (TEM)	55
3.3.4	Atomic Force Microscopy (AFM)	56
3.3.5	Raman Spectroscopy	57
3.4	Optical Characterization	58
3.4.1	Ultraviolet-Visible (UV-VIS) Spectroscopy	58
3.4.2	Photoluminescence (PL) Spectroscopy	59
	CHAPTER 4: RESULTS AND DISCUSSION	60
4.1	Introduction	60
4.2	Glass Series Containing Monometallic Titanium Nanoparticles	61

4.2.1 Physical Properties	61
4.2.2 X-Ray Diffraction (XRD) Spectroscopy	63
4.2.3 Ultraviolet-Visible (UV-VIS) Spectroscopy	64
4.2.3.1 Absorbance Spectra	64
4.2.3.2 Plasmon Peak for Titanium NPs	64
4.2.3.3 Direct Optical Energy Band and Indirect Optical Energy Band	65
4.2.4 Fourier-Transform Infrared (FTIR) Spectroscopy	68
4.2.5 Transmission Electron Microscopy (TEM)	70
4.2.6 Atomic Force Microscopy (AFM)	73
4.2.7 Photoluminescence (PL) Spectroscopy	74
4.3 Glass Series Containing Bimetallic Titanium and Aluminium Nanoparticles	79
4.3.1 Physical Properties	79
4.3.2 X-Ray Diffraction (XRD) Spectroscopy	81
4.3.3 Ultraviolet-visible (UV-VIS) Spectroscopy	81
4.3.3.1 Plasmon Peaks for Titanium and Aluminium NPs	82
4.3.3.2 Direct Optical Energy Band and Indirect Optical Energy Band	83
4.3.4 Fourier-Transform Infrared (FTIR) Spectroscopy	86
4.3.5 Transmission Electron Microscopy (TEM)	87
4.3.6 Atomic Force Microscopy (AFM)	92
4.3.7 Photoluminescence (PL) Spectroscopy	93
4.3.8 Raman Spectroscopy	95
CHAPTER 5: CONCLUSION	100
5.1 Introduction	100
5.2 Conclusion	100
5.3 Future Outlook	101
REFERENCES	102
APPENDIX	120

LIST OF TABLES

	Page
Table 3.1: Glass composition containing monometallic titanium NPs and erbium content with composition of $(70-x-y)\text{TeO}_2-20\text{ZnO}-9\text{Na}_2\text{O}-1\text{Er}_2\text{O}_3-(x)\text{TiO}_2-(y)\text{Al}_2\text{O}_3$, where $x = 0.0, 0.1, 0.2, 0.3, 0.4$ and 0.5 mol% and $y = 0$ mol%	50
Table 3.2: Glass composition containing bimetallic titanium NPs, aluminium NPs and erbium content with composition of $(70-x-y)\text{TeO}_2-20\text{ZnO}-9\text{Na}_2\text{O}-1\text{Er}_2\text{O}_3-(x)\text{TiO}_2-(y)\text{Al}_2\text{O}_3$ where $x = 0.0$ and 0.3 mol% and $y = 0.0, 0.1, 0.2, 0.3, 0.4, 0.5$ and 0.6 mol%	50
Table 3.3: Glass composition containing monometallic titanium NPs without erbium content with composition of $(70-x-y)\text{TeO}_2-20\text{ZnO}-9\text{Na}_2\text{O}-0\text{Er}_2\text{O}_3-(x)\text{TiO}_2-(y)\text{Al}_2\text{O}_3$, where $x = 0.0, 0.1, 0.2, 0.3, 0.4$ and 0.5 mol% and $y = 0$ mol%	51
Table 3.4: Glass composition containing bimetallic titanium NPs and aluminium NPs without erbium content with composition of $(70-x-y)\text{TeO}_2-20\text{ZnO}-9\text{Na}_2\text{O}-0\text{Er}_2\text{O}_3-(x)\text{TiO}_2-(y)\text{Al}_2\text{O}_3$ where $x = 0.0$ and 0.3 mol% and $y = 0.0, 0.1, 0.2, 0.3, 0.4, 0.5$ and 0.6 mol%	51
Table 4.1: Direct energy band gap (E_{dir}), indirect energy band gap (E_{ind}) and Urbach energy (E_{U}) of glass containing monometallic NPs	68
Table 4.2: IR band assignments for respective glass samples	69
Table 4.3: Size of titanium NPs in longitudinal and transverse axis and determination of aspect ratio in TZNETi0.3 glass sample	72
Table 4.4: Glass code, composition and surface roughness for TZNETi0.3 glass sample	74
Table 4.5: Area under the graph for emission spectra	77
Table 4.6: PL enhancement factor for emission spectra	78

Table 4.7:	Direct energy band gap (E_{dir}), indirect energy band gap (E_{ind}) and Urbach energy (E_U) of glass containing bimetallic NPs	85
Table 4.8:	IR band assignments for respective glass samples	87
Table 4.9:	Size of bimetallic titanium and aluminium NPs in longitudinal and transverse axis and determination of aspect ratio in TZNETiAl0.3 glass sample	89
Table 4.10:	Size of bimetallic titanium and aluminium NPs in longitudinal and transverse axis and determination of aspect ratio in TZNETiAl0.6 glass sample	91
Table 4.11:	Glass code, composition and surface roughness of TZNETiAl0.6 glass sample	92
Table 4.12:	Area under the graph for emission spectra	95
Table 4.13:	PL enhancement factor for emission spectra	95
Table 4.14:	Spectral region and Raman band assignments and bonding vibrations	97
Table 4.15:	Area under the graph for Raman spectra	98
Table 4.16:	Enhancement factor for Raman spectra	98



UMS
UNIVERSITI MALAYSIA SABAH

LIST OF FIGURES

	Page
Figure 2.1: Victoria and Albert museum overview of Merovingian glass 5 th to 6 th century	9
Figure 2.2: The atomic arrangement of amorphous glass and solid quartz.	10
Figure 2.3: V-T diagram of glass transition where T_M is the melting point of glass and T_G is glass transition temperature.	11
Figure 2.4: Structural units of tellurite represents by Q_m^n , where n is the number of bridging oxygen and m is the number of bonded oxygen atoms.	12
Figure 2.5: Presentation of structural units in tellurite glass. The left structure is the trigonal bipyramidal TeO_4 , centre is the distorted trigonal bipyramidal TeO_{3+1} and the right side is the trigonal pyramidal TeO_3	13
Figure 2.6: Glass network structure when TeO_2 is added with Na_2O	14
Figure 2.7: Glass network structure when TeO_2 is added with Zn	15
Figure 2.8: Lanthanides ion in group 3 of the periodic table	16
Figure 2.9: Different shapes of bimetallic NPs in a shape of (a) octahedral nanocage, (b) cubic nanocage, (c) octahedral dendritic hollow, (d) cubic dendritic hollow, (e) core-shell octahedral dendritic, (f) core-shell cubic dendritic	20
Figure 2.10: Structures of bimetallic (a) mixed alloys, (b) random alloys, (c) two interface sub-cluster, (d) three interface sub-cluster, (e) small A-B bonds sub-cluster, (f) core-shell NPs, (g) multi shell core-shell NPs, (h) small cores coated by single shell, (i) free-moving core within hollow shell	21
Figure 2.11: (a) The NPs dispersed in a porous material undergoes Ostwald ripening which larger particles are grow to the expense of smaller particles. (b) During Ostwald ripening process, the particles growth is either stopped, (c) or they	22

	continue to grow at which the red arrow shows the pressured particles that support the continuous growth	
Figure 2.12:	Schematic diagram of coalescence process	23
Figure 2.13:	Mechanism for excitation of localized surface plasmon resonance (LSPR)	24
Figure 2.14:	SERS effect on silver surface	25
Figure 2.15:	Schematic illustration of Bragg's Law	27
Figure 2.16:	XRD spectra of EZT glasses	28
Figure 2.17:	XRD spectra for TSWD glass system	29
Figure 2.18:	XRD spectra of TEA glasses	29
Figure 2.19:	Instrumentation of Fourier-transform	30
Figure 2.20:	FTIR spectra for $(ZnO)_x [(TeO_2)_{0.7} - (PbO)_{0.3}]_{1-x}$ glass system	31
Figure 2.21:	Jablonski diagram showing processes of Rayleigh and Raman scattering	32
Figure 2.22:	Raman spectra of TZNE and TZNETi samples	34
Figure 2.23:	Raman spectra of AlTe glasses	35
Figure 2.24:	(a) A sharpened probe scanning across the surface and is monitored to generate a 2D line profile. (b) The scanned line profile is combined to generate a 3D surface image	36
Figure 2.25:	Working principle of AFM	37
Figure 2.26:	Graph of force against distance	38
Figure 2.27:	Topography of glass surface roughness with SiO ₂ concentration (a) 0.00 mol %, (b) 0.05 mol %, (c) 0.10 mol %, (d) 0.15 mol % and (e) 0.20 mol %	39
Figure 2.28:	(a) TEM image of TiO ₂ and (b) lattice fringe pattern of TiO ₂	40
Figure 2.29:	TEM images of (a) Au-TiO ₂ nanocluster and (b) Ag-TiO ₂ annealed at 500 °C	41
Figure 2.30:	Electromagnetic spectrum for visible region	42
Figure 2.31:	Absorption spectra for TZNE and TZNETi glasses	43
Figure 2.32:	Optical band gap of titanium	45
Figure 2.33:	Urbach energy of titanium	46

Figure 2.34:	Photoluminescence spectra for TLZNE glass	48
Figure 3.1:	Carbolite CWF 1200 furnace for glass melting process	52
Figure 3.2:	Schematic diagram for XRD characterization	53
Figure 3.3:	Schematic diagram for infrared characterization	55
Figure 3.4:	Schematic diagram for TEM imaging	56
Figure 3.5:	Schematic diagram for surface roughness characterization	57
Figure 3.6:	Schematic diagram for Raman characterization	58
Figure 3.7:	Schematic diagram for UV-VIS	59
Figure 3.8:	Schematic diagram of Fluorescence Spectrophotometer	60
Figure 4.1:	Glass samples without erbium content with varying concentration of TiO ₂ ranging from 0 mol% to 0.5 mol%	62
Figure 4.2:	Glass samples with erbium content and varying concentration of TiO ₂ ranging from 0 mol% to 0.5 mol%	63
Figure 4.3:	XRD pattern of glass samples with varying TiO ₂ content	63
Figure 4.4:	UV-Vis absorption spectra in the range of 380-1100 nm	64
Figure 4.5:	SPR band positions for titanium NPs	65
Figure 4.6:	Plot of $(\alpha\hbar\omega)^2$ against photon energy $\hbar\omega$ for direct band gap measurement	66
Figure 4.7:	Plot of $(\alpha\hbar\omega)^{1/2}$ against photon energy $\hbar\omega$ for indirect band gap measurement	66
Figure 4.8:	Plot of $\ln(\alpha)$ against photon energy $\hbar\omega$ for Urbach energy measurement	67
Figure 4.9:	IR spectra of glass samples with varying concentration of titanium NPs	69
Figure 4.10:	(a) TEM image of TZNETi0.3 glass sample and (b) Electron diffraction of respective glass sample	71
Figure 4.11:	Lattice fringe pattern of TZNETi0.3 glass sample	73
Figure 4.12:	3D Surface topography for TZNETi0.3 glass sample	74
Figure 4.13:	Excitation spectra of glass samples	75
Figure 4.14:	Emission spectra of glass samples	76

Figure 4.15:	Partial energy level diagram of Er^{3+} ion showing UC emission at 547 nm and 668 nm through GSA (ground state absorption) and NR (non-radiative decay)	78
Figure 4.16:	Glass samples without erbium content with varying concentration of Al_2O_3 ranging from 0.1 mol% to 0.6 mol%	80
Figure 4.17:	Glass samples with erbium content and varying concentration of Al_2O_3 ranging from 0.1 mol% to 0.6 mol%	80
Figure 4.18:	XRD spectra of glass with varying Al_2O_3 concentration	81
Figure 4.19:	UV-Vis absorption spectra for glass containing bimetallic NPs	82
Figure 4.20:	SPR band positions for titanium (554 nm) and aluminium (827 nm) NPs	83
Figure 4.21:	Plot of $(\alpha\hbar\omega)^2$ against photon energy $\hbar\omega$ for direct band gap measurement	84
Figure 4.22:	Plot of $(\alpha\hbar\omega)^{1/2}$ against photon energy $\hbar\omega$ for indirect band gap measurement	84
Figure 4.23:	Plot of $\ln(\alpha)$ against photon energy $\hbar\omega$ for Urbach energy measurement	85
Figure 4.24:	IR spectra of glass samples with varying concentration of aluminium NPs	86
Figure 4.25:	(a) TEM image of TZNETiAl0.3 glass sample and (b) Electron diffraction of respective glass sample	88
Figure 4.26:	Lattice fringe pattern of TZNETiAl0.3 glass sample	89
Figure 4.27:	(a) TEM image of TZNETiAl0.6 glass sample and (b) Electron diffraction of respective glass sample	90
Figure 4.28:	Lattice fringe pattern of TZNETiAl0.6 glass sample	91
Figure 4.29:	3D surface topography of TZNETiAl0.6 glass sample	92
Figure 4.30:	Excitation spectra of glass samples	93
Figure 4.31:	Emission spectra of glass samples	94
Figure 4.32:	Deconvoluted peak for TZNE glass samples	96
Figure 4.33:	Raman spectra for glass samples with varying concentration of Al_2O_3	96

LIST OF ABBREVIATIONS

AFM	-	Atomic Force Microscopy
BO	-	Bridging Oxygen
EFAD	-	Electric Field Assisted Diffusion
ET	-	Energy Transfer
FTIR	-	Fourier-Transform Infrared
GSA	-	Ground State Absorption
LSPR	-	Localized Surface Plasmon Resonance
NBO	-	Non-Bridging Oxygen
NPs	-	Nanoparticles
NR	-	Non-Radiative Decay
PL	-	Photoluminescence
RE	-	Rare Earth
SAED	-	Selected Area Electron Diffraction
SERS	-	Surface Enhance Raman Scattering
SP	-	Surface Plasmon
SPR	-	Surface Plasmon Resonance
SR	-	Surface Roughness
TEM	-	Transmission Electron Microscopy
UC	-	Up-Conversion
UV	-	Ultra-violet
UV-VIS	-	Ultraviolet-visible
XRD	-	X-Ray Diffraction

LIST OF SYMBOLS

%T	-	Transmittance
Δx	-	Length of deflection
B	-	Constant for extended tailing band
C_a	-	Concentration of absorption
E_{dir}	-	Direct band gap energy
E_{ind}	-	Indirect band gap energy
E_u	-	Urbach energy
F	-	Force
I	-	Incident beam
I_o	-	Transmitted beam
T_c	-	Cooling temperature
T_G	-	Glass transition temperature
T_M	-	Melting point temperature
b	-	Path length
d	-	Spacing of crystal plane
e	-	Natural logarithms base
hω	-	Function of photon energy
i	-	Square root of -1
k	-	Constant
n	-	Order of reflection
t	-	Time
v	-	Frequency
$\alpha\omega$	-	Absorption coefficient
θ	-	Angle
λ	-	Wavelength
ω	-	Photon frequency

LIST OF APPENDIX

	Page
Appendix A1: List of Publication	120



UMS
UNIVERSITI MALAYSIA SABAH

CHAPTER 1

INTRODUCTION

1.1 Background of Study

Glass architectural is plain and simply aesthetically in human eyes. This versatile material is used in everyday applications, from homes to kitchenware, automobiles, decorations and down to several unseen applications such as electronics, medical equipment, insulator and reinforcement material. Types of glass are made according to their specific needs and applications. The engineering of glass is made to exhibit different kind of structural, optical, thermal and chemical properties (Shelby, 2005).

The most common glasses used in the commercial glass industry are borosilicate and soda-lime silicate. Borosilicate-based glass are commonly found in the exterior lighting, industrial and lab equipment as they are high durability and its superior thermal shock resistance (Hasanuzzaman *et al.*, 2016). Food and drinks beverage and container, accessories and decorative tableware are made from soda-lime silicate-based glass, basically almost 80% of world-wide production due to its inexpensive cost and easy to be made as they have relatively low melting point (Ashby, 2012). Meanwhile, there is another type of glass which an interesting smart material in non-crystalline solids research has been reported. Tellurite glass as the most stable oxide has opened a whole new photonics world to the interest of researchers such as optical amplifiers, lasers utilizing tellurite-based glass gain media, solar energy harvesting, biomedical applications, optical sensing and more applications (El-Mallawany, 2018). The trigonal bipyramid structure of tellurium dioxide gives it the advantage to form different bonds with different ions which enable it to be tune to favourable material properties for photonic application (Gulenko *et al.*, 2014).

Metallic nanoparticles (NPs) and tellurite glass have recently grown in research on the optical and luminescence enhancement properties. This glass preparation is study along with the presence of rare-earth ion due to the energy transfer mechanism from the metallic NPs to the rare-earth ion which will be contributed to the intensified local field and luminescence enhancement (de Almeida, 2008). The local field effect induced by the surface plasmon resonance (SPR) of metallic NPs which is yield in the vicinity of rare-earth ion is investigated extensively due to its stimulating effect in intensified Raman signal, or also known as surface-enhanced Raman scattering (SERS). These metallic NPs are called as the SERS substrate for which they possess the favourable properties as a plasmonic material.

SERS is initially founded in 1970 by Fleischmann and co-workers when they reported an unusually large Raman signal is obtained from pyridine adsorbed on a roughened silver electrode (Fleischmann *et al.*, 1974). Since then, SERS has been exploited mostly in biomedical and biochemical research which provide new combination and techniques for analytical applications. However, some issues should be taken into consideration before SERS is fully taken into bio-clinical practices such as reproducibility, background interference signal and qualitative analysis. The convergence of photonics and nanoscience creating more opportunities on producing SERS substrate that is significant on detecting wider range of biological or chemical analytes (Candeloro *et al.*, 2017).

Few experiments have been demonstrated with incorporation of monometallic NPs in tellurite glass. In previous work demonstrated by Amjad et al (2013), the embedment of silver NPs shows significant Raman signal up to the power of tenth along with enhancement in photoluminescence due to the local field effect of silver NPs (Amjad *et al.*, 2013). Another experiment is conducted with incorporation of gold NPs in tellurite glass resulting in SERS enhancement which is highly potential candidate for solid state lasers and other nanophotonic devices (Ghoshal *et al.*, 2015). A similar experimental work was performed by Saidi et al (2018), in which the enhancement of Raman signal is observed in the tellurite glass with the presence of bimetallic NPs of silver and titanium. Hence, it is proved the combination of bimetallic NPs potentially improves the absorption, optical and structure properties better than monometallic NPs due to the attributed localized surface plasmon resonance of Ag/Ti

which transferred the strong local electric field to the rare-earth ions positioned in their vicinity (Saidi *et al.*, 2018).

This current research proposed a new idea of producing a simple and cheaper nanostructured plasmonic glass which exerts the SERS capabilities for molecular detection application by using conventional melt-quenching technique. The direct embedment of metallic NPs into glass composition by using a melt-quenching technique provides facile glass fabrication which possesses beneficial features for SERS application. The other technique of fabricate nanostructured plasmonic glass such as ion-exchange, chemical vapour deposition and laser-induced plasma required multiple steps and involves an intricate process. In current research, the selection of titanium and aluminium as bimetallic NPs is prerequisite due to their plasmonic properties in the ultraviolet (UV) region which give rise to the Localized Surface Plasmon Resonance (LSPR) on the surface of metallic NPs.

1.2 Problem Statement

In order to identify the molecular structure of a molecule, the vibrational information of the molecule must be extracted. This is possible with the aid of Raman spectroscopy. Raman spectroscopy is a method to analyse the molecular and vibrational properties of a molecule in a non-contact and non-destructive ways (Vašková *et al.*, 2011). In this modern developing century, the established technique of Raman spectroscopy is constantly used in chemical and materials analysis (Ochsenkuhn *et al.*, 2012). However, Raman spectra signal is not strong enough to be applicable in wide biomedical field and biomolecular sensing application (El-Said *et al.*, 2017).

In order to overcome this limitation, this research proposes the embedment of metallic NPs in the glass matrix to allow the amplification of Raman spectra up to the factor of 10^5 . The amplification in Raman spectra with the aid from metallic NPs is known as surface-enhanced Raman spectroscopy (SERS) (Sharma, 2012). In this research, two series of glasses containing monometallic and bimetallic NPs were prepared by using conventional melt-quenching technique. Further, the surface morphology, structural and optical properties of each glass is characterized in-depth